similar results as presented in Figures 3 and 4. Figure 5 shows the measured peak antenna gain for operating frequencies across the 2.4-GHz and 5.2-GHz bands. The peak antenna gain ranges from about 4.5–6.2 dBi for the 2.4-GHz band (2400–2484 MHz), and from about 4.3–5.5 dB for the 5.2 GHz band (5150–5350 MHz).

4. CONCLUSION

Novel design of a dual-band dipole antenna printed on an FR4 substrate to achieve diversity operation in the 2.4-GHz and 5.2-GHz bands for a WLAN access point has been proposed. A constructed prototype has also been successfully implemented, and two separate wide resonant modes covering the 2.4-GHz and 5.2-GHz WLAN bands have been obtained. In addition, the measured radiation patterns of the antenna's two operating ports are directional in two complementary half spaces, which make the WLAN access point capable of performing spatial diversity to combat the multipath interfering problem and enhance system performance.

REFERENCES

1. Y.H. Suh and K. Chang, Low cost microstrip-fed dual frequency printed dipole antenna for wireless communications, Electron Lett 36 (2000), 1177–1179.
2. S.N. Tsai, Antenna module for portable computer, US Patent No. 6297779, Oct. 2, 2001.

EXPERIMENTAL RESULTS FOR A CW-MODE OPTICALLY CONTROLLED MICROWAVE SWITCH ON A SILICON-BASED COPLANAR WAVEGUIDE

Sangil Lee, Yasuo Kuga, and Ruth Ann Mullen
Department of Electrical Engineering
University of Washington
Box 352500
Seattle, WA 98195-2500

Received 14 August 2002

ABSTRACT: *A CW-mode optically controlled microwave switch (CW-mode OMS) on a coplanar waveguide (CPW) for both a standard and a new design with carrier-confinement structure is investigated. We experimentally show that it may not be possible to obtain less than 7 dB of insertion loss with the standard OMS, and the carrier diffusion limits the improvement of insertion loss in CW-mode operation. We present a new design with a carrier-confinement structure with silicon (Si) substrate etching to confine the optically generated free-carriers. Less than 2 dB of insertion loss is obtained with the new carrier-confined OMS.*
 Microwave Opt Technol Lett 36: 257–262, 2003; Published online in Wiley InterScience (www.interscience.wiley.com). DOI 10.1002/mop.10737

Key words: *optical control; microwave switch; coplanar waveguide; CW lasers; photoconductivity*

1. INTRODUCTION

Optical control has been emphasized in microwave devices due to unique advantages such as fast response, immunity from EMI, high power handling, good isolation between controlling and controlled devices, and possibilities for monolithic integration with other devices [1]. Since the reporting of picosecond photoconductivity, various microwave devices using the photoconductivity effect have been developed. One simple application for the photoconductivity effect is the direct excitation of a gap on a semiconductor transmission line with a laser light. The transmission characteristics can be controlled with the generated free carriers; the ON and OFF states can be used for a switching device or an attenuator. Initially, picosecond switches using pulse laser sources were developed as very useful techniques [2]. Intensive research in this field led to the demonstration of various microwave devices using the photoconductivity effect. In recent years, CW- or quasi-CW mode optically controlled microwave devices have also been an area of growing interest for novel devices, such as optically reconfigurable antenna arrays [3, 4]. However, adverse influences are observed in the CW-mode operations. The number of generated free carriers may not increase in proportion to the incident optical power in the very high power range. Thus, obtaining higher photoconductivity may not be possible even though the incident optical power is increased in CW-mode operation [5, 6].

In a very low duty pulse-mode OMS, the pulse duration is much shorter than the recombination rate, and the carrier recombination can be ignored in counting the number of optically generated free-carriers. Thus, a direct bandgap material such as GaAs, which has a very short recombination rate, can be effectively used to reduce switching speed. However, in the CW-mode operation, the number of optically generated free-carriers is directly related to the recombination rate of the substrate material. In the steady state, the number of optically generated free-carriers is given by [5]:

$$\Delta n = \frac{\alpha I(\omega)}{h\omega}(1 - R)S\tau, \tag{1}$$

where α is the absorption coefficient, $I(\omega)$ is light intensity, $h\omega$ is the photon energy to excite electrons, R is the surface reflectivity, S is the relative spectral response of the semiconductor material exhibiting a peak response at λ_0, and τ is the recombination rate or carrier lifetime. Although Eq. (1) neglects some phenomena such as surface recombination and carrier diffusion, it provides a basis for the selection of a substrate material. In general, a substrate with a longer lifetime can maintain a higher free-carrier density at the expense of switching speed. This will restrict the choice of the substrate material to an indirect bandgap material such as a Si wafer for the CW-mode operation, and the diffusion length of the optically generated free-carriers will become longer with a longer lifetime [7]. Therefore, it is expected that the physical confinement of the free-carriers will be important to improve insertion loss, which can be done by Si substrate etching. In this paper, various effects due to the CW-mode operation are investigated analytically and experimentally, and the best-case insertion loss for both a standard and a new carrier-confined CW-mode OMS is presented.

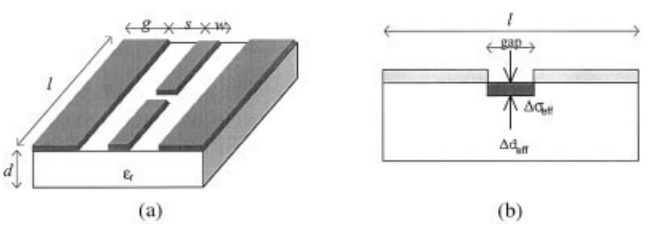

Figure 1 A basic design of the CW-mode OMS: (a) CPW on an Si wafer with a gap on a signal line; (b) simulation model with effective plasma depth and effective photoconductivity

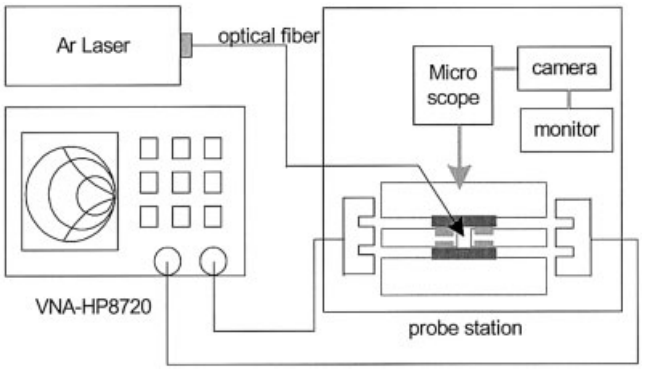

Figure 2 An experimental setup for the transmission coefficient measurement

2. A STANDARD CW-MODE OMS

2.1. Experimental Results

The basic structure of a standard CW-mode OMS is shown in Figure 1 [7]. For the given parameters which include the dielectric constant ($\varepsilon_r = 11.9$ for high resistivity Si wafer) of a substrate material, substrate thickness ($350 \sim 400$ μm) and micro-probe pitch size (200 μm), the CPW line width and the line separation between the signal line and the ground plane are determined to obtain 50Ω CPW. The 120-μm signal line width with different gap widths (0, 25, 50, and 75 μm gaps) is designed to study the effects of the gap size, and four different line separations from 50 μm to 80 μm are considered to keep the 50Ω line, depending on the different substrate thickness to be used later for the carrier-confinement structure. Other parameters used for the design are line length $l = 3.5$ mm and ground width $g = 0.8$ mm.

A simple micro-fabrication technique is applied to make CPW line patterns on a high resistivity ($> 4000\Omega$ cm), float-zone, $\langle 100 \rangle$ Si wafer. First, a mask pattern is designed to be used for a selective deposition or a selective etching process. Then, CPW metal patterns are created using photolithography. Cr and Au are deposited for 200 Å and 5000 Å, respectively using an E-beam evaporator. A metal wet etching technique is used for obtaining the CPW line patterns. The experimental setup for the transmission coefficient measurements is shown in Figure 2. An Ar laser ($\lambda = 488$ nm) is used for an optical power source to excite the gap area, and the light is guided through the multi-mode optical fiber. The transmission characteristics are measured with a vector network analyzer (HP8720D) and a 3D microwave probe station at a frequency range from 500 MHz to 20 GHz. All the measurements are "thru" calibrated with a reference line having no gap. Hence, insertion loss can be read directly from the plot.

First, insertion loss for the different gap sizes is measured and the measured results are shown in Figure 3. The optical power used for the measurements is 3 mW, which is measured at the tip of the optical fiber. Thus, the actual optical power incident into the gap area and the optical power density is approximately 1 mW and 265 mW/mm^2, respectively. As shown in Figure 3(a), the insertion loss with the 25-μm gap is approximately 10 dB, which is 8 dB lower than that of the 75-μm gap sample. However, as shown in Figure 3(b), the ON/OFF difference is not significantly different between the 25-μm and 75-μm gap samples, and it varies 10 to 35 dB, depending on the frequency. Generally, a smaller gap sample shows lower insertion loss. However, if the gap size is too small, it may not be able to obtain a high enough ON/OFF ratio. Based on this experiment, a 25-μm gap provides both low insertion loss and high ON/OFF ratio. Therefore, we use the 25-μm gap sample for the best-case insertion loss measurements. Figure 4 shows the measured insertion loss in the high optical power range up to 30 mW. As we expect, the insertion loss becomes less and the ON/OFF ratio increases with the higher optical power, but they are saturated. From the measurements, -8 dB of the best-case insertion loss is obtained for the standard CW-mode OMS with the 25-μm gap sample. The optical power used for the measurement is approximately 10 mW. This result suggests that it is not possible to obtain close to 0 dB of insertion loss with the standard CW-mode OMS only with an increase of the incident optical power.

2.2. Analysis with Numerical Simulations

To analyze the experimental results, the transmission characteristics of the CW-mode OMS are simulated using a finite element code high frequency structure simulator (HFSS). The model used for the simulation is based on the effective photoconductivity and the effective plasma depth of the gap region [5] without considering carrier diffusion. Hence, we can compare the measured insertion loss when carrier diffusion is involved, to the simulation results without considering carrier diffusion. Therefore, the difference of the insertion loss due to the carrier diffusion can be observed.

The number of optically generated free-carriers on the substrate surface can be obtained from Eq. (1), which does not consider the

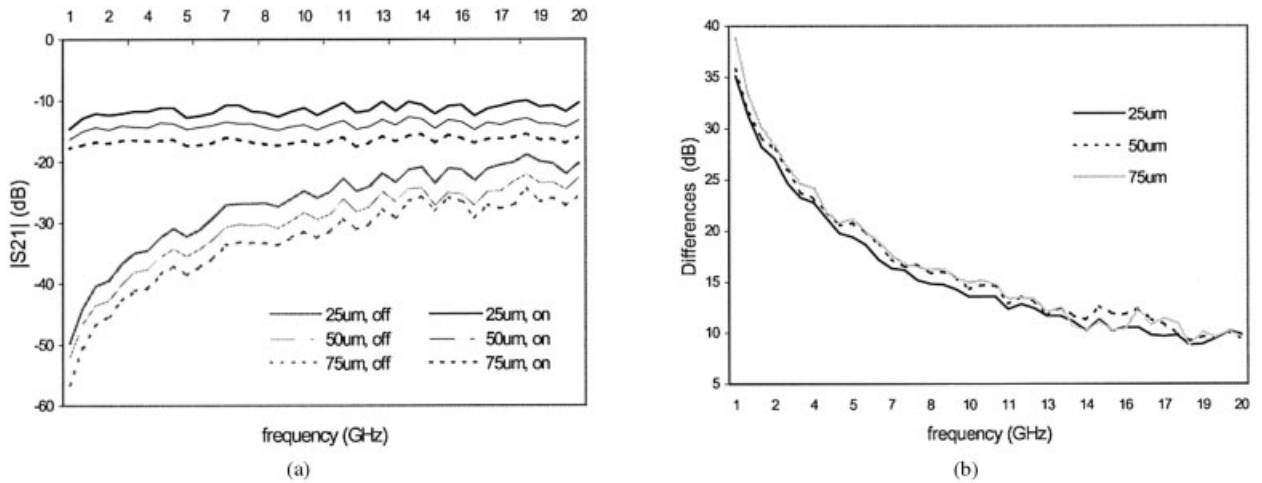

Figure 3 Measurement results for a different gap size as a function of frequency at 3 mW: (a) insertion loss; (b) ON/OFF difference

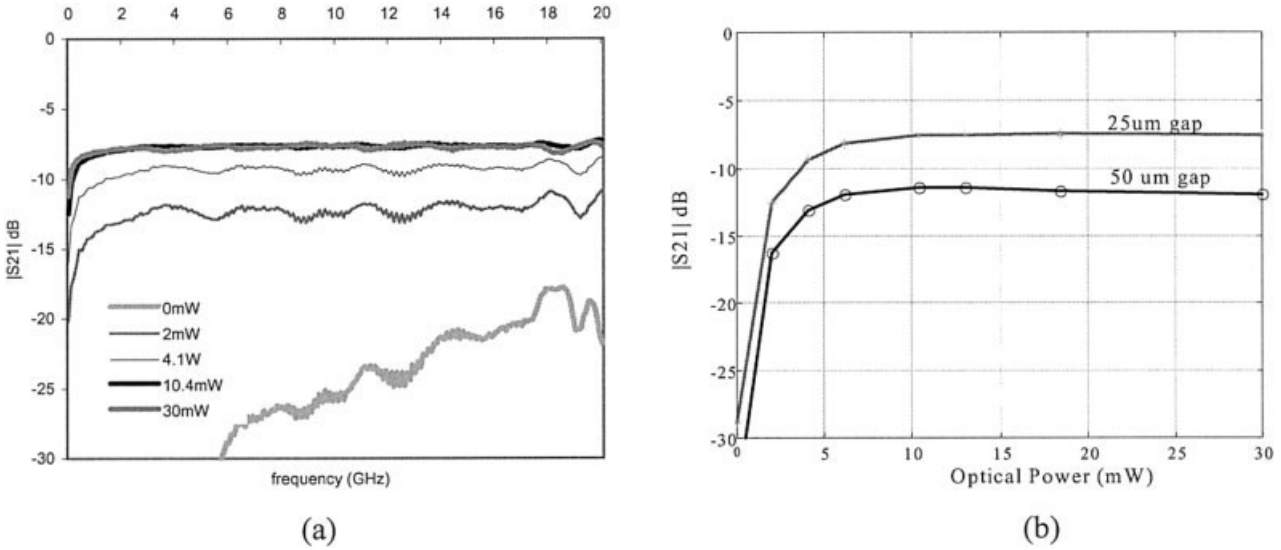

Figure 4 Measurement results for the best-case insertion loss with a 25-μm gap sample: (a) as a function of frequency; (b) as a function of incident optical power at 6 GHz for both 25-μm and 50-μm gap samples

carrier diffusion process. The photoconductivity due to the generated free-carriers is expressed by [5]:

$$\Delta\sigma_0 = q\Delta n(\mu_n + \mu_p), \tag{2}$$

where q is the electrical charge, Δn is the number of optically generated free-carriers, and μ_n and μ_p are the mobilities of electrons and holes, respectively. However, the photoconductivity is exponentially decreased, as shown in Figure 5(a). To make this problem simple, we suppose that the effective photoconductivity and the effective plasma depth is the same as $\Delta\sigma_0$ and $1/\alpha$, respectively, as shown in Fig. 5(a). From Eqs. (1) and (2), $\Delta\sigma_0$ is 5×10^6 S/m with 880 mW/mm^2 of the incident optical power density, which corresponds to 10 mW optical power with a 120 μm beam diameter, and the plasma depth is 1 μm. This result shows that the gap region becomes a good conductor with the given condition. Other quantities used for the calculation are: $\alpha = 1 \times 10^4$ cm^{-1}, $\tau = 10^{-4}$ sec, $S = 0.5$, and $R = 0.3$. Close to 0 dB of the insertion loss is obtained from the HFSS simulations with $\Delta\sigma_0 = 5 \times 10^6$ S/m. As a result, the optical power used for obtaining 8 dB of the best-case insertion loss is high enough to obtain close to 0 dB of insertion loss if carrier diffusion can be ignored. Based on this experiment, it is found that carrier diffusion is one of the main reasons for the bad insertion loss in the CW-mode operation, and we expect the improvement of the insertion loss with a proper carrier confinement structure to block the diffusion of the carriers out through the substrate.

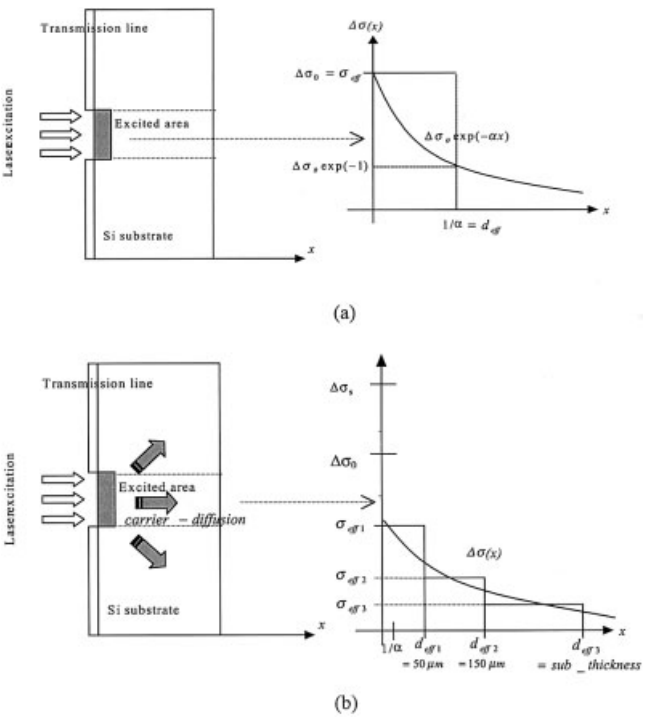

Figure 5 Induced photoconductivity as a function of depth: (a) from the silicon surface without considering a carrier-diffusion; (b) effective photoconductivity and the plasma depth with consideration of carrier-diffusion [5]

3. A NEW CARRIER-CONFINED CW-MODE OMS

3.1. Basic Ideas

The basic carrier confining idea is to make grooves around the gap area, which can be implemented by Si substrate etching. Figure 6(a) shows the proposed groove design with two separated regions. One pattern is located between the ground plane and the signal line around the gap area (dark gray), and the other pattern is on the signal line (bright gray). The most efficient way to confine the carriers is an encapsulation of the exciting area with the air gap produced by the substrate etching, but it may not be a possible process without the disconnection of the signal line. Thus, we can make etching patterns only partially on the signal line for further confinement. If we make a narrower signal line, we can confine more carriers, but there will be more reflections at the narrower signal line due to impedance change, especially at the high frequency range. However, numerical simulation results showed that the loss due to the narrower signal line was less than 0.5 dB, which may not be significant. Another way to confine the carriers is to minimize the substrate thickness. The thickness of the Si wafers we use is approximately 380 μm. Although we confine the carriers horizontally, there is large space to diffuse out to the bottom. Therefore, it is expected that a thinner substrate can confine the carriers more effectively. The thinner substrate can be obtained

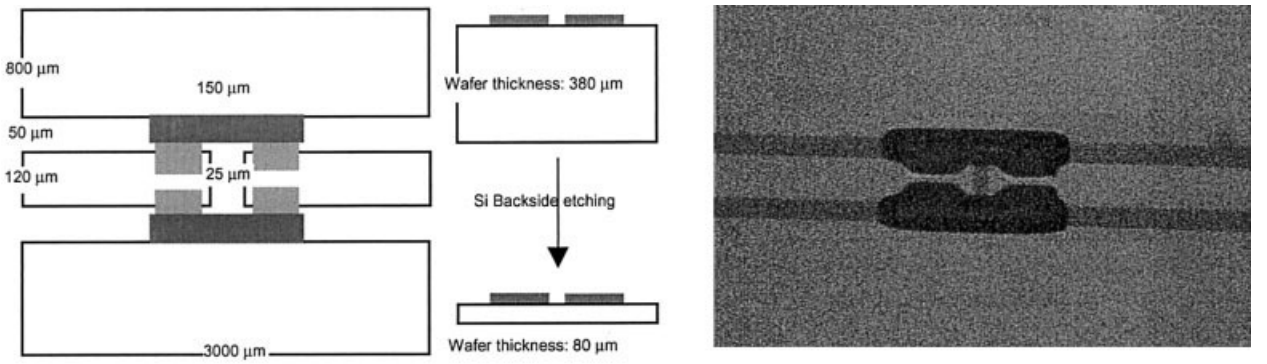

Figure 6 A new design for a carrier-confined OMS: (a) a schematic diagram; (b) a picture of the fabricated sample with a new carrier-confinement structure

with backside etching of the substrate after the final process step. However, a depth of less than 50 μm may be too thin to handle the next step based on our experience.

A silicon dioxide layer on an Si surface provides both advantages and disadvantages for the insertion loss of the CW-mode OMS. First, a silicon dioxide layer can be effectively used to reduce the surface recombination rate because the silicon dioxide layer diminishes the band split phenomenon at the surface, which increases the carrier lifetime and the number of generated free-carriers [8]. Another advantage of the silicon dioxide layer is low reflectivity at the surface, due to the anti-reflection coating effect. The optimum thickness for zero reflectivity is 2300 Å. However, silicon dioxide has a very high thermal resistivity, which may cause a heat dissipation problem, and we need to optimize the silicon dioxide thickness. A silicon dioxide layer is thermally deposited, and the thickness is controlled by the BOE etching before the device fabrication to observe the effect of the oxide thickness.

3.2. Experimental Results

The same micro-fabrication technique explained in section 2 is applied to make the CPW line patterns. However, a second photolithography for the etching pattern and reactive ion etcher (RIE) Si etching is needed. Also, silicon dioxide is thermally deposited before starting the process to observe the insertion loss according to the silicon dioxide thickness. Figure 6(b) shows the picture of the fabricated sample with the grooves etched out for more than 40 μm. The actual etching areas are larger than the designed areas. We use a dry etching technique with a Trion RIE, which has undercutting problems due to the isotropic Si etching. Therefore, this undercutting problem should be considered in the etching pattern design.

Several samples are fabricated and tested to observe insertion loss, depending on the silicon dioxide thickness and the confining structure. First, we measure insertion loss for the different silicon dioxide thicknesses at 6 mW with 25-μm gap samples. As we expect, there is significant improvement of insertion loss with the silicon dioxide layer, but the improvement becomes weaker as the silicon dioxide layer becomes thicker. As shown in Figure 7, insertion loss can be optimized with the very thin silicon dioxide layer at approximately 100 Å. Figure 8(a) shows the measured insertion loss for both with and without carrier-confinement technique as a function of frequency at 20 mW of incident optical power. Only the carrier-confined OMS is fabricated with a thin silicon dioxide layer, and all the insertion loss differences in between, with and without a confinement structure, include the improvement due to the silicon dioxide layer. Insertion loss is improved less than 1 dB each with the grooves in between the ground plane and the signal line, and the other grooves on the signal line. However, when the vertical confinement is employed with the substrate etching, the insertion loss can be reduced substantially. The minimum substrate thickness that we can handle is approximately 80 μm, which is used for the measurement. Furthermore, we expect lower than 2 dB of insertion loss for a lower optical power, if a thinner substrate (less than 50 μm) is possible with an advanced fabrication technique such as selective backside etching. Figure 8(b) shows another measured insertion loss as a function of incident optical power at 6 GHz. When insertion loss is improved linearly with a higher optical power up to 5 mW, the improvement is decreased, however, it is not saturated with the carrier-confinement structure. Hence, it may be possible to obtain lower than 2 dB of insertion loss with much higher incident optical power, although it is not a good way to improve the insertion loss. Finally, less than 2 dB of insertion loss is obtained with the new carrier-confinement structure.

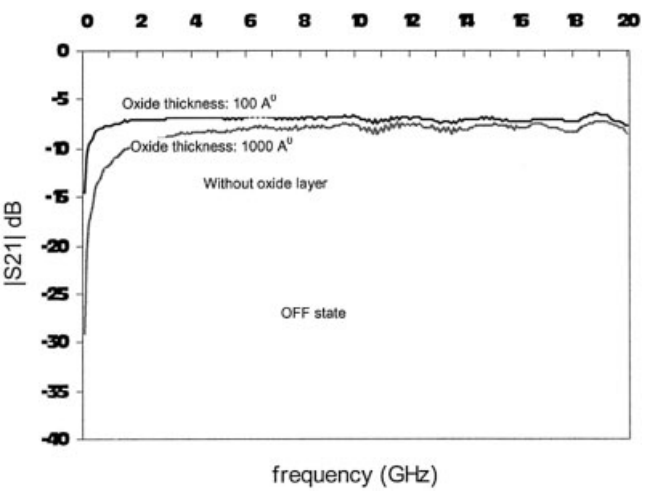

Figure 7 Measurement results for a different silicon dioxide thickness as a function of frequency at 6 mW with a 25-μm gap sample

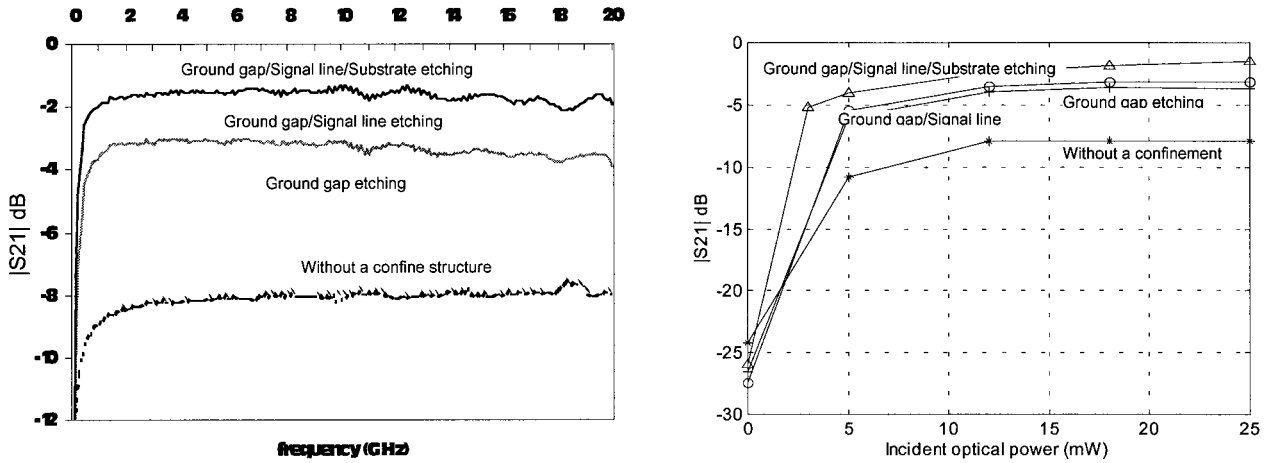

Figure 8 Measurement results of the best-case insertion loss with the various carrier-confinement structures with the 25-μm gap sample: (a) as a function of frequency at 20-mW optical power; (b) as a function of incident optical power at 6 GHz

3.3. Analysis with Simulation Results

Effective photoconductivity and plasma depth for the CW-mode operation are well defined and derived in [5], and we are able to estimate effective photoconductivity of the gap region with the given effective plasma depth. Another way to obtain effective photoconductivity is an inverse method using the measured insertion loss and the numerical simulation results. As shown in Figure 9, 8 dB of insertion loss corresponds to the 550 S/m of the effective photoconductivity for the defined plasma depth from the surface, as shown in Figure 5(b). In the CW-mode operation, the plasma depth is longer than the thickness of the given substrate. To obtain more correct effective photoconductivity, the substrate is separated into three regions from the substrate surface, and each region has different photoconductivity. The 550 S/m corresponds to the top layer. The effective photoconductivity of the second and third layers are 440 and 352 S/m, respectively. Also, the effective photoconductivity for the carrier-confined OMS is obtained from the inverse method, which is not available from [5] due to the different structure. As shown in Figure 9, the effective photoconductivity with the carrier-confined OMS is approximately 3000 S/m for 50 μm of the effective plasma depth, which is the thickness of the thinner substrate. Based on this experiment, more than five times higher effective photoconductivity can be obtained with the new carrier-confined structure and the thin silicon dioxide layer.

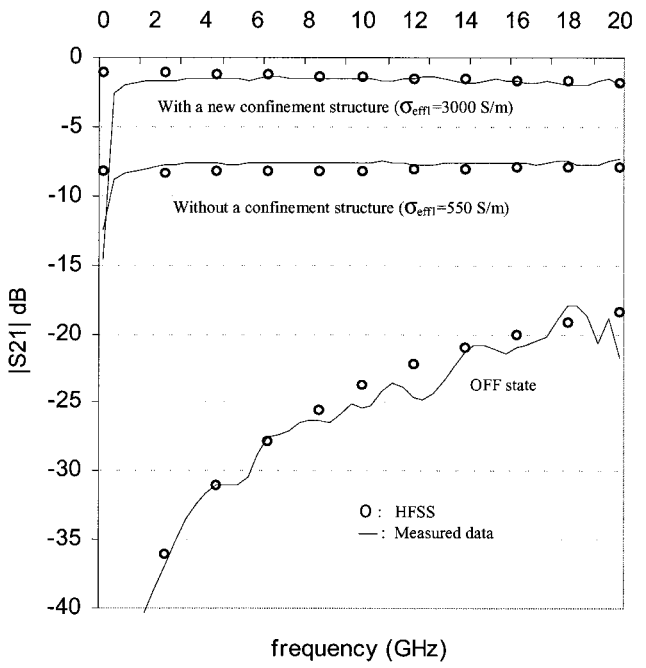

Figure 9 HFSS simulation results compared to the measured insertion loss for both a standard and a carrier-confined OMS

4. CONCLUSION

We have investigated the CW-mode OMS for both a standard and a new carrier-confined structure. First, a standard OMS has been characterized with the measured insertion loss. It has been found that there is a limitation for improving the insertion loss only with an increase of an incident optical power. The main reason for the poor insertion loss on the CW-mode OMS is very long carrier diffusion length. The best-case insertion loss obtained from the measurements was approximately 8 dB. Therefore, the new design with a carrier confinement structure, which is implemented by Si substrate etching, has been proposed. As a result, less than 2 dB of the insertion has been obtained with the new design.

In our present study, the laser light is coupled through an optical fiber placed close to the gap. This is not an optimum method to deliver optical energy to the gap region. With the improved coupling method, we expect that the efficiency of OMS will be enhanced.

ACKNOWLEDGEMENT

This work was supported by the National Science Foundation (grant ECS-9908849) and the U.S. Office of Naval Research (grant N00014001027).

REFERENCES

1. C.H. Lee, Picosecond optics and microwave technology, IEEE Trans Microwave Theory Tech MTT-38 (1990), 596–607.
2. A.M. Johnson and D.H. Auston, Microwave switching by picosecond photoconductivity, IEEE J Quantum Electron QE-11 (1975), 283–287.
3. E.W. Jacobs, D.W. Fogliatti, H. Nguyen, D.J. Albares, C.T. Chang, and C.K. Sun, Photo-injection p-i-n diode switch for high-power RF switching, IEEE Trans MTT-50 (2002), 413–419.
4. J.L. Freeman, B.J. Lamberty, and G.S. Andrews, Optoelectronically

reconfigurable monopole antenna, Electronics letters 28, (1992), 1502–1503.
5. W. Platte, Effective photoconductivity and plasma depth in optically quasi-CW controlled microwave switching devices, IEE Proceedings 135 (1988).
6. W. Platte and B. Sauerer, Optically CW-induced losses in semiconductor coplanar waveguides, IEEE Trans Microwave Theory and Tech MTT-37 (1989), 139–149.
7. S. Lee and Y. Kuga, Optically CW-mode controlled microwave switches with carrier-confinement on a coplanar waveguide, 2001 IEEE Antennas & Propagation Society Int Symp Dig 2 (2001), 514–517.
8. D.A. Neamen, Semiconductor physics & devices, 2nd edition, Irwin, 1997.

CONCENTRATOR AND LENS MODELS FOR CALCULATING THE IMPULSE RESPONSE ON IR-WIRELESS INDOOR CHANNELS USING A RAY-TRACING ALGORITHM

Silvestre Rodríguez Pérez,[1] Rafael Pérez Jiménez,[2] Oswaldo B. González Hernández,[1] José Alberto Rabadán Borges,[2] and Beatriz Rodríguez Mendoza[1]
[1] Dpt. Física Fundamental y Experimental Electrónica y Sistemas
Universidad de La Laguna, Spain
[2] Dpt. de Señales y Comunicaciones
Universidad de Las Palmas de Gran Canaria, Spain

Received 7 August 2002

ABSTRACT: *This paper presents concentrator and lens models for the detector and emitter, respectively, upon which a Monte Carlo ray-tracing algorithm allows the evaluation of impulse response on infrared (IR) wireless indoor channels. We also present computer simulation results that show the effects of concentrator FOV and reception direction on the impulse response, received optical power, and channel rms delay spread, which allow us to propose structures for angle-diversity receivers.* © 2003 Wiley Periodicals, Inc. Microwave Opt Technol Lett 36: 262–267, 2003; Published online in Wiley InterScience (www.interscience.wiley.com). DOI 10.1002/mop.10738

Key words: *ray tracing; impulse response; infrared channel; CPC; angle-diversity*

1. INTRODUCTION

The overall performance of an indoor wireless infrared (IR) link is closely related to the degree of directionality of its transmitters and receivers, and their respective orientation. Various link designs have been proposed and analyzed in [1]. Directed line-of-sight links (LOS) are usually very power efficient and relatively free from multipath distortion. Such links, however, require alignment of the transmitter at the *y* receiver and are very sensitive to blockage. In contrast to LOS links, nondirected non-line-of-sight links (non-LOS), often called diffuse links, are highly robust against blockage and do not require aiming. On the other hand, the diffuse links are subject to a high path loss and multipath distortion. One option to compensate for path loss is to increase the transmit power, which is not always possible due to power consumption considerations and eye-safety regulations.

In [2, 3], a nondirected non-LOS architecture based upon utilization of an angle-diversity receiver and a multibeam transmitter has been reported. An angle-diversity receiver utilizes multiple receiving elements that are oriented in different directions. It can be used in place of a single-element receiver in either LOS or non-LOS links. In a conventional angle-diversity receiver, each receiving element utilizes its own nonimaging concentrator, such as a compound parabolic concentrator (CPC). A principal advantage of angle-diversity reception is that it allows the receiver to simultaneously achieve high optical gain and a wide field of view (FOV). Moreover, an angle-diversity receiver can reduce the impact of ambient light noise, path loss, co-channel interference, and multipath distortion, in part by exploiting the fact that they are often received from directions different than that of the desired signal. The advantages achieved depend on how the signals received in the different elements are detected and processed. For this reason, the use of a simulation tool is necessary in order to study the influence of the infrared (IR) channel and propose new techniques and receiver structures for those systems.

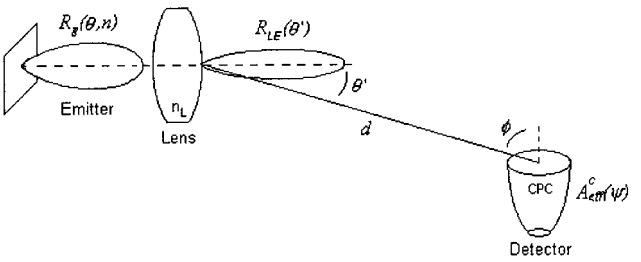

Figure 1 Geometry of emitter and detector, without reflectors

The characteristics of the room where the IR channel is implemented determine some features of the communication, such as multipath dispersion and path loss. For fixed emitter and receiver locations, multipath dispersion and path loss are completely characterized by the impulse response. To evaluate this response, a simulation tool for the fast calculation of the impulse response on IR wireless indoor channels has been presented in [4, 5]. In these works, we have used Phong's model to approximate the reflection pattern of the indoor surfaces upon which a Monte Carlo ray-tracing algorithm allows us to evaluate the impulse response. In this paper, lense and nonimaging-concentrator models are presented. In contrast to previous works [1, 2, 6], where an idealized concentrator with a constant gain within its FOV and a null propagation delay are used, a new concentrator model is proposed. In this model, the reflection losses and propagation delay, introduced by the concentrator, are considered.

In the next sections the Monte Carlo ray-tracing algorithm is described and the lense and concentrator models are presented. Finally, several simulation results are reported in order to discuss the effects of concentrator FOV and direction on the impulse response, the received optical power, and the channel rms delay spread [1, 2].

ALGORITHM DESCRIPTION

For the calculation of the impulse response of the IR indoor channel the line-of-sight and multiple-bounce impulse responses are considered.

Line-of-Sight Impulse Response. Given an emitter *E* and a detector *R* with lens and CPC, respectively, in an environment without reflectors (Fig. 1), with a large distance *d* between both relative to detector size, the power received is approximately